Structural Transition of Poly[(*R*)-3-hydroxybutyrate-*co*-(*R*)-3-hydroxyvalerate] Single Crystals on Heating As Revealed by Synchrotron Radiation SAXS and WAXD

Tomoharu Sawayanagi,[†] Toshihisa Tanaka,[‡] Tadahisa Iwata,[‡,||] Hideki Abe,[†,‡] Yoshiharu Doi,[†,‡] Kazuki Ito,[§,⊥] Tetsuro Fujisawa,[§] and Masahiro Fujita*[,‡,#]

Department of Innovative and Engineered Materials, Tokyo Institute of Technology, Nagatsuta 4259, Midori-ku, Yokohama 226-8502, Japan; Polymer Chemistry Laboratory, RIKEN Institute, Hirosawa 2-1, Wako-shi, Saitama 351-0198, Japan; and Biometal Science Laboratory, RIKEN SPring-8 Center, Kouto 1-1-1, Sayo-cho, Sayo-gun, Hyogo 679-5148, Japan

Received December 27, 2006; Revised Manuscript Received February 9, 2007

ABSTRACT: The annealing behavior of poly[(*R*)-3-hydroxybutyrate-*co*-(*R*)-3-hydroxyvalerate] (P(3HB-*co*-3HV)) crystal was studied by synchrotron radiation small-angle X-ray scattering (SAXS) and wide-angle X-ray diffraction (WAXD). Solution-grown single crystals of P(3HB-*co*-3HV) with various composition of 3HV (5.3−16.0 mol %) were used in order to examine the effect of 3HV unit on the structural changes on heating. The two-dimensional (2D) SAXS patterns demonstrated that the lamellar thickness of P(3HB-*co*-3HV) single crystal starts to increase discontinuously at an annealing temperature and that two populations with two different thicknesses of original and reorganized crystals coexist in a temperature range, independent of 3HV composition. This fact means that the 3HV unit with longer side chain does not hinder the jump of lamellar thickness. The 2D WAXD and differential scanning calorimetric experiments indicated that the discontinuous thickening is caused by partial melting and recrystallization. The depression of transition temperature from the original crystal to the thicker one and the incompletion of reorganization with increase in 3HV unit can be attributed to the lowering of the interaction between the copolymer chain stems and to the difficulty in incorporation of the chains to crystal lattice, respectively.

Introduction

Thermal behavior of polymer crystals has been investigated to reveal molecular motion in the solid states below their melting points. An increase of the lamellar thickness on heating has been widely studied by many researchers. However, there still exist two main mechanisms that have been proposed to explain the thickening process from years ago: One is the sliding diffusion mechanism that polymer chains in the lamellar crystal slide through the crystal lattice along the chain axis,[1] and the other is that the lamellar crystals once melt and then turn to thicker ones by recrystallization.[2]

In recent years, the morphological changes of various polymer crystals on heating have been followed in real-time using atomic force microscopy (AFM) with a hot stage, and the dynamic structural changes for the isolated crystals have been visually provided in detail.[3−9] To follow in real time the fast dynamic structural changes during annealing such as lamellar thickening process, synchrotron radiation X-ray is also of advantage because the small-angle X-ray scattering (SAXS) and wide-angle X-ray diffraction (WAXD) measurements can be made in a very short time frame. Furthermore, these provide fine details on the structural changes from the molecular scale up to the macroscale events such as changes in lamellar morphology. So far, the thermal behaviors of various polymer and oligomer crystals such as polyethylene (PE),[10,11] ultralong alkanes,[12−14] poly(aryl ether ketones),[15] syndiotactic polypropylene,[16] and oligo-3-hydroxybutyrate (3HB)[17,18] have been investigated by synchrotron radiation X-ray scattering. In low-molecular-weight oligomeric chains, the quantized nature of lamellar thickening due to chain unfolding has been of interest because this property helps the mobility of the polymer during its lamellar thickening to be understood.[12−14,17,18] In the case of ultralong alkanes ($C_{102}H_{206}$− $C_{294}H_{590}$), the chain unfolding or the lamellar thickening is accompanied by both the contraction of unit cell and the reduction and recovery in WAXD intensity which is associated with melting and recrystallization.[14] In a recent study on thickening process of oligo-3HB crystal by the combination of synchrotron radiation SAXS and WAXD, it has been proposed that the thickening of oligo-3HB crystal occurs via partial melting and recrystallization.[18] For higher molecular weight polymers, the molecular motion of PE in its crystal during annealing was examined by Rastogi et al. using a synchrotron radiation SAXS and Raman spectroscopy.[10] They reported that PE crystal exhibits a doubling of lamellar thickening, which is similar to the discontinuous nature of lamellar thickening in oligomer crystals.[10] This thickening mechanism has been explained by the chain sliding diffusion mechanism.[10] Besides PE crystal, the similar discontinuous thickening for polyamide and polypivalolactone crystals was previously reported.[1,19,20]

Recently, we reported the real-time synchrotron radiation two-dimensional (2D) SAXS and WAXD studies on the thermal behavior of poly[(*R*)-3-hydroxybutyrate] (P(3HB)) single crystals.[21,22] The P(3HB) single crystal shows a discontinuous lamellar thickening with the orientation of chain axis maintained. Owing to the synchrotron radiation X-ray coupled with a CCD

* To whom all correspondence should be addressed: Tel +81-48-467-9403; Fax +81-48-462-4667; e-mail mfujita@riken.jp.
† Tokyo Institute of Technology.
‡ RIKEN Institute.
§ RIKEN SPring-8 Center.
|| Present address: Sciences of Polymeric Materials, Department of Biomaterial Sciences, Graduate School of Agricultural and Life Sciences, The University of Tokyo.
⊥ Present address: Structural Materials Science Laboratory, RIKEN SPring-8 Center.
Present address: Bioengineering Laboratory, RIKEN Institute.

10.1021/ma062957d CCC: $37.00
Published on Web 03/13/2007

Table 1. Molecular Characteristics of P(3HB-*co*-3HV)

sample	$M_n \times 10^{-4}$	M_w/M_n
P(3HB-*co*-5.3 mol % 3HV)	1.61	1.33
P(3HB-*co*-10.9 mol % 3HV)	1.89	1.30
P(3HB-*co*-16.0 mol % 3HV)	2.04	1.29

camera, which can be recorded within tens of milliseconds, it was clearly observed that two populations of the original and the reorganized crystals coexist while the former decreases and the latter increases in the transition. It was also found that the discontinuous thickening occurs at higher temperatures upon increasing the original lamellar thickness.[22] The crystallinity, estimated from the 2D WAXD patterns, first decreased and then recovered during the thickening. In addition, the lamellar thickening was accompanied by endo- and exothermic signals in differential scanning calorimetry (DSC). Therefore, we have proposed that the discontinuous lamellar thickening of P(3HB) single crystals is caused by partial melting and recrystallization.[21,22]

For further understanding the mechanism of the discontinuous thickening of P(3HB) single crystals, it is of interest to investigate the effect of chemical regularity on the discontinuous thickening. P(3HB) is a family of poly(hydroxyalkanoate)s (PHAs) produced by a number of bacteria. Among PHAs, poly-[(*R*)-3-hydroxybutyrate-*co*-(*R*)-3-hydroxyvalerate] (P(3HB-*co*-3HV)) is one of the most familiar P(3HB) copolymers,[23] and the structural studies on P(3HB-*co*-3HV) crystals have been extensively performed as well as those on P(3HB) homopolymer crystals.[24−31] It has been suggested that P(3HB-*co*-3HV) forms a characteristic crystal structure in contrast to the other P(3HB) copolymers. Bluhm et al. first reported that, for the samples of 3HV content up to 30 mol %, the 3HV units are accommodated in the P(3HB) crystal lattice accompanied by a small lateral expansion of the unit cell; that is, P(3HB-*co*-3HV) crystal exhibits isomorphism.[25] Afterward, some structural models on isomorphism of P(3HB-*co*-3HV) crystal have been considered.[26,29,30]

In this study, we examined the annealing behavior of the P(3HB-*co*-3HV) solution-grown single crystals with various composition of 3HV (5.3−16.0 mol %) by synchrotron radiation SAXS and WAXD. In addition, the thermal properties of the single crystals were characterized by DSC. Comparing with the thermal behavior of P(3HB) single crystals reported previously, we discussed the effect of 3HV unit on the structural changes during the discontinuous thickening.

Experimental Section

Materials. Bacterial P(3HB-*co*-3HV) random copolymer was purchased from Aldrich Co. The molecular weight of P(3HB-*co*-3HV) used here was dropped to 20 000−15 000 by alkaline hydrolysis according to the same procedure in our previous works.[21,22] After the alkaline hydrolysis, the sample was fractionated to obtain P(3HB-*co*-3HV) with a narrow composition distribution of 3HV by the following procedure:[31] P(3HB-*co*-3HV) (2 g) was first dissolved in 200 mL of chloroform, and *n*-heptane was added with stirring at room temperature until the solution became turbid. The solution was further stirred at 35 °C for 1 h and then left at room temperature for 24 h. The suspension was centrifuged, and the first precipitate was then collected by removing supernatant. To the supernatant solution, 20 mL of *n*-heptane was further added, and the solution was stirred for 1 h. After the solution was further left for 24 h at room temperature, the second precipitate was collected. The latter procedures, the addition of *n*-heptane (20 mL) to the supernatant and the collection of precipitate, were repeated until the addition of any amount of *n*-heptane caused no precipitation. Finally, the residual polymer sample in the solution was collected by precipitation into methanol and vacuum filtration. Each precipitate was dried under vacuum. The 3HV content of each fractionated P(3HB-*co*-3HV) was determined by ^{1}H NMR (JNM-AL300, JEOL, Japan), estimating the integral intensity ratio of two spectra attributed to the methyl resonances of 3HB and 3HV units.[24,31] The number-average molecular weight (M_n) and polydispersity (M_w/M_n) of the P(3HB-*co*-3HV) samples were determined by gel-permeation chromatography (10A GPC system, Shimadzu, Japan). The 3HV content, M_n, and M_w/M_n of the fractionated P(3HB-*co*-3HV) samples used here are shown in Table 1.

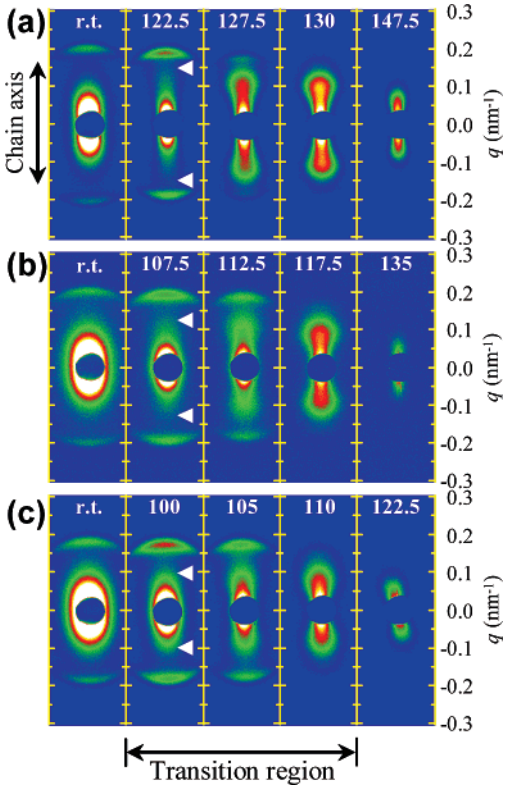

Figure 1. 2D SAXS patterns of sedimented single-crystal mats of P(3HB-*co*-3HV) containing (a) 5.3, (b) 10.9, (c) 16.0 mol % 3HV on heating at 10 °C/min. The meridian corresponds to the chain axis as indicated with the vertical arrow. These patterns were taken at the temperatures indicated in the images. The arrowheads indicate a set of new scattering peak.

Preparation of Solution-Grown Single Crystals and Their Sedimented Mats. Solution-grown single crystals of P(3HB-*co*-3HV) were grown isothermally at 60 °C for 24 h in a 0.05% w/v 1-octanol solution. The sedimented single-crystal mats were obtained by filtration after the suspension was cooled down to room temperature and then dried under vacuum.

Synchrotron Radiation SAXS and WAXD Measurements. Real-time SAXS and WAXD measurements were carried out in the BL45XU beamline (wavelength, $\lambda = 0.09$ nm) at SPring-8, Harima, Japan. The camera lengths in the SAXS and WAXD measurements were set to be about 2200 and 150 mm, respectively. Sample-heating device was set in the beamline station.[21,22] The heating unit was remotely controlled from outside the shielding hutch. The single-crystal mats were set in the sample holder and heated from room temperature to around 180 °C at a heating rate of 10 °C/min. All 2D SAXS and WAXD patterns were recorded with a CCD camera (C7300-10-12NR, Hamamatsu Photonics, Japan) coupled with an X-ray image intensifier (V5445P MOD, Hamamatsu Photonics, Japan). The pixel size of CCD camera is 125 μm × 125 μm. The exposure times in the SAXS and WAXD were determined in such a way that intensity signals were not saturated during the course of experiment for any individual samples (22−151 and 51−227 ms, respectively).

Data Analysis of SAXS and WAXD. The procedures of data analyses of SAXS and WAXD patterns were the same as those in

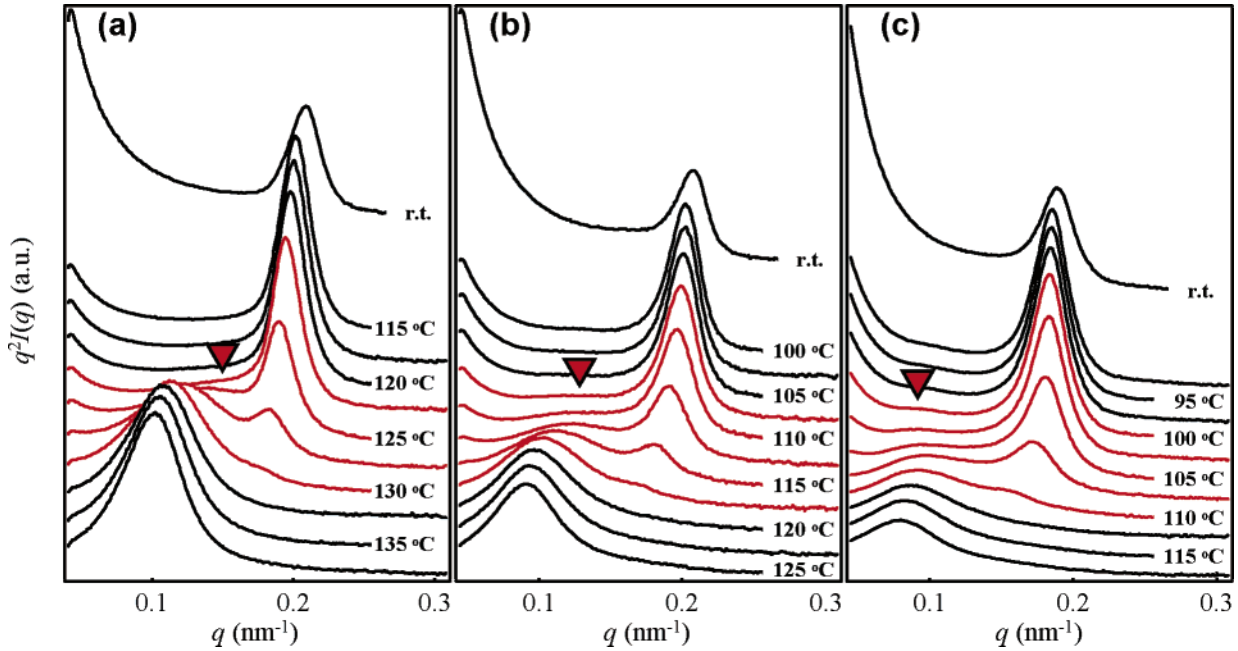

Figure 2. Lorentz corrected 1D profiles derived from 2D SAXS patterns of single-crystal mats of P(3HB-*co*-3HV) containing (a) 5.3, (b) 10.9, and (c) 16.0 mol % 3HV. The profiles during the lamellar thickening are highlighted with red lines. The arrowhead in each figure indicates the scattering peak from reorganized crystals.

our previous studies on the annealing behavior of P(3HB) homopolymer single crystals.[21,22] As shown below, the scattering peaks in the 2D SAXS patterns are arced, indicating that the orientation of the sedimented single-crystal mats distributes. To extract the structural information on the whole system, thus, the 2D SAXS images were converted to one-dimensional (1D) profiles by circularly averaging, as described in ref 32, with a Rigaku R-AXIS Display software package. The averaging over the whole azimuthal angle was performed. Subsequently, the Lorentz correction was applied to the azimuthal-average 1D profiles after subtraction of background. The individual scattering peak in the 1D profile was fitted by Gaussian function with IGOR Pro 4 software package (WaveMetrics, Inc.). From the fitting parameters obtained, the long period and the scattering peak area were calculated. The unit lattice dimensions (*a*-, *b*-, and *c*-axes) and the apparent crystallite sizes (D_{200}, D_{020}, and D_{002}) were calculated from the peak positions and the widths of 200, 020, and 002 reflections, which parameters were obtained from the fitting of Gaussian function, on the equatorial and meridian line scans in the 2D WAXD images. The apparent crystallite sizes were calculated according to Scherrer's equation without any corrections including deconvolution of instrumental broadening. For the estimation of overall crystallinity, the 2D WAXD images were converted to the integrated 1D profiles by the same procedure in SAXS analysis. Each of the crystalline peaks and amorphous scattering was fitted by Gaussian function, and then the total area of crystalline peaks (A_c) and of the amorphous background (A_a) were calculated using the fitting parameters obtained.

Differential Scanning Calorimetry. Thermal properties of P(3HB-*co*-3HV) single crystals were evaluated by DSC (Pyris 1, Perkin-Elmer Inc.) of the sedimented single-crystal mats. The DSC thermograms were obtained under a nitrogen atmosphere at a heating rate of 10 °C/min, which was the same rate as that in the synchrotron radiation X-ray measurements.

Results and Discussion

SAXS Measurements. Real-time synchrotron radiation SAXS measurements on heating at 10 °C/min were performed for sedimented mats of solution-grown single crystals of P(3HB-*co*-3HV) containing 5.3, 10.9, and 16.0 mol % 3HV. The 2D SAXS patterns were taken at elevated temperatures every 10 °C rise in temperature up to around 90 °C and thereafter every 2.5 °C. A part of the 2D SAXS image series for each single crystal is shown in Figure 1. In this figure, the meridian corresponds to the lamellar stacking direction in the sedimented mats. A set of scattering peaks from the stacking periodicity of as-grown-single crystals was recognized on the meridian. The integrated 1D profiles are shown in Figure 2. At the vicinity of beam stopper, the scattering intensity increased steeply upon decreasing angle in the 1D profiles obtained at room temperature. This is probably associated with voids between poorly stacked lamellar packets.[13] From the 1D profiles, the long periods at room temperature were estimated as 4.8 nm (q = 0.208 nm^{-1}), 4.8 nm (q = 0.207 nm^{-1}), and 5.3 nm (q = 0.189 nm^{-1}) for 5.3, 10.9, and 16.0 mol % of 3HV unit, respectively (here, $q = 2 \sin\theta/\lambda$, 2θ = scattering angle). For sedimented single-crystal mats, the long period is regarded as one lamellar thickness, viz. fold period, in contrast to the bulk sample.

At an annealing temperature (T_a), a new set of scattering peaks was observed at a lower angle for any content of 3HV, as indicated with the arrowheads in Figures 1 and 2, while the original peaks, whose position little shifted inward on heating up to just below the T_a, remained. Namely, the discontinuous increase in long period occurs at the T_a as well as P(3HB) homopolymer single crystal.[21,22] The new scattering peaks were clearly recognized at q = 0.150 nm^{-1} at T_a = 122.5 °C for 5.3 mol % 3HV, q = 0.129 nm^{-1} at 107.5 °C for 10.9 mol % 3HV, and q = 0.091 nm^{-1} at 102.5 °C for 16.0 mol % 3HV. The long periods estimated from the new scattering peaks at the T_a were 6.7, 7.8, and 11.0 nm for 5.3, 10.9, and 16.0 mol % 3HV, respectively. Two populations with the different long periods could be detected up to T_a = ~130, 117.5, and 110 °C for 5.3, 10.9, and 16.0 mol % 3HV, respectively, as shown in Figures 1 and 2. After the transition of discontinuous increase, the remaining peak shifted to low angles and finally diminished due to the complete melting.

Figure 3 shows the plots of the long period and the scattering peak area against T_a. These values were extracted from all integrated 1D SAXS profiles acquired in this study. In this figure, the changes of the long period and the scattering peak

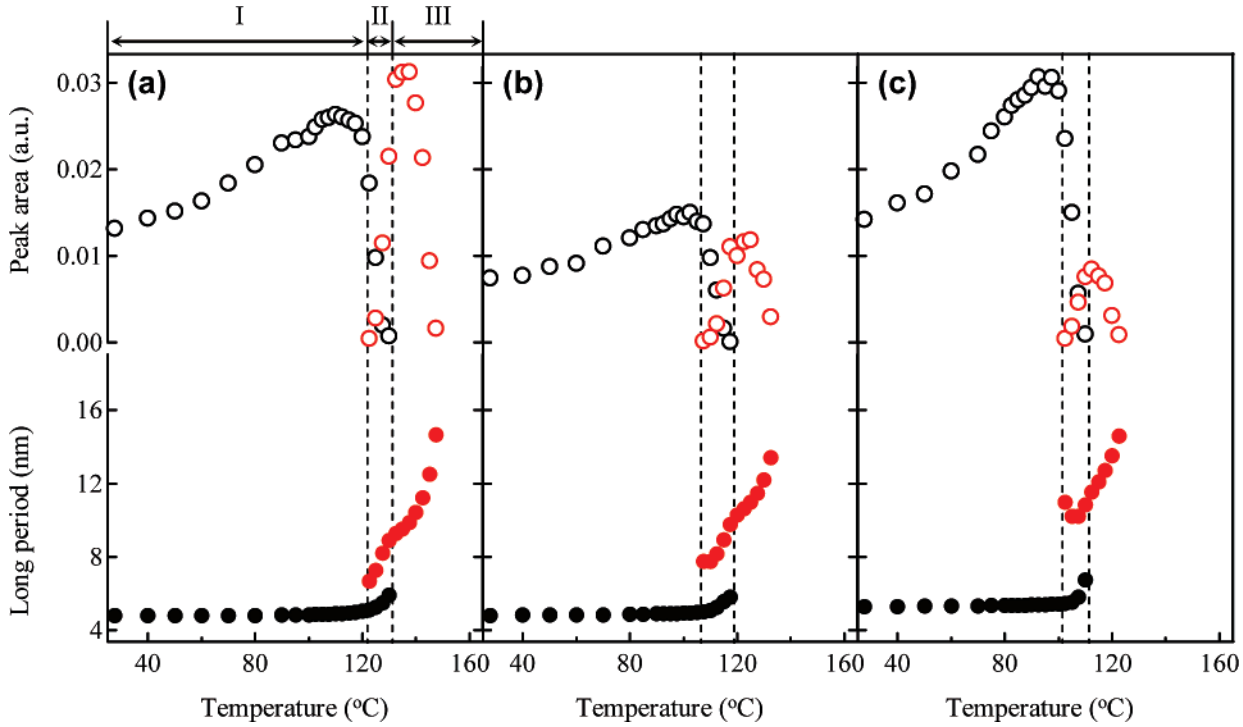

Figure 3. Temperature dependence of SAXS peak area (open symbol) and long period (filled symbol) from initial crystal (black) and reorganized crystal (red) for single-crystal mats of P(3HB-*co*-3HV) containing (a) 5.3, (b) 10.9, and (c) 16.0 mol % 3HV.

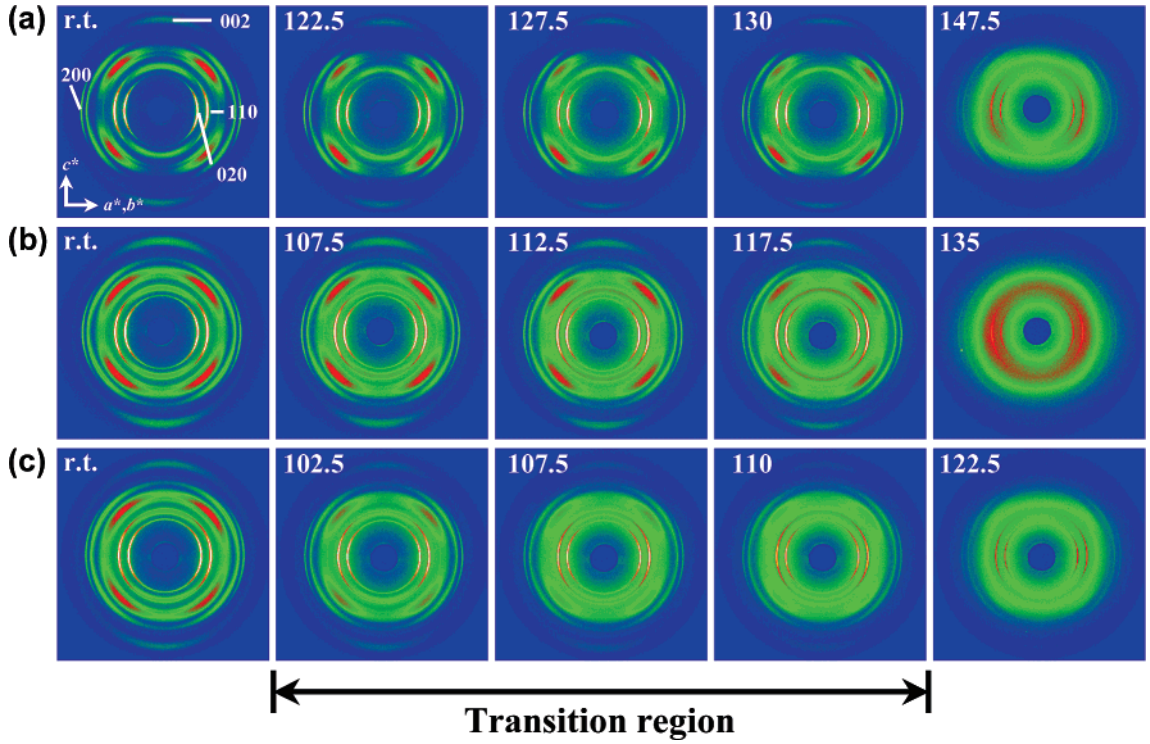

Figure 4. 2D WAXD patterns of sedimented single-crystal mats of P(3HB-*co*-3HV) containing (a) 5.3, (b) 10.9, and (c) 16.0 mol % 3HV on heating at 10 °C/min. These patterns were taken at the temperatures indicated in the images.

area can be classified into three regions.[21,22] Regions I, II, and III correspond to the temperature ranges up to the onset of, during, and after the discontinuous thickening, respectively. The gradual increase of scattering area in region I is probably due to the increase in the difference of electron density between crystalline (core) and noncrystalline (fold parts of chains and cilia) regions with temperature. The change of the area in region II indicates that the mass of reorganized crystals increases while that of original ones decreases with temperature. Namely, the reorganization progresses in turn from the thinner crystals among the original population. After the transition region, the long period of reorganized crystals increased whereas the scattering peak area from the reorganized crystals decreased. This indicates that the increase of long period in this region is caused by increase of amorphous phase due to melting rather than further lamellar thickening of reorganized crystals.[33]

WAXD and DSC Measurements. Real-time synchrotron radiation WAXD measurements at 10 °C/min were also

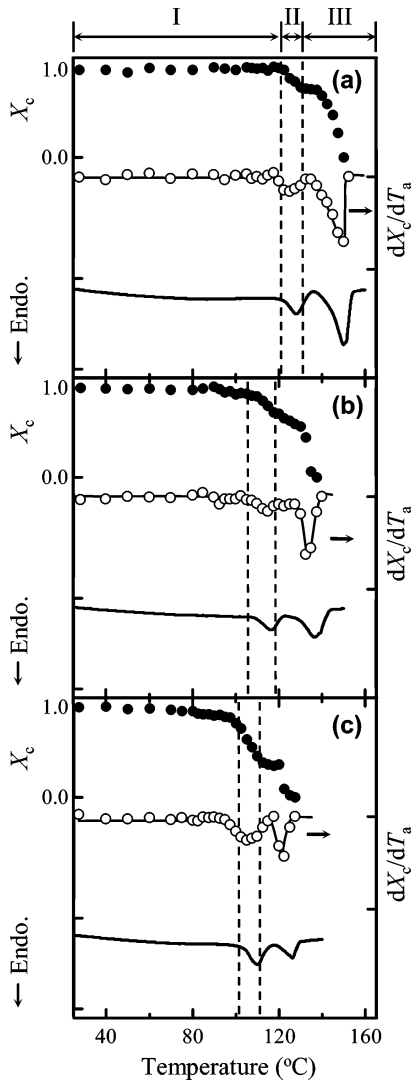

Figure 5. Relative crystallinity X_c, differential X_c with respect to T_a, and DSC curve as a function of temperature: (a) 5.3, (b) 10.9, and (c) 16.0 mol % 3HV.

performed for the sedimented mats of solution-grown P(3HB-*co*-3HV) single crystals containing 5.3, 10.9, and 16.0 mol % of 3HV unit, respectively. A part of the 2D WAXD image series for each P(3HB-*co*-3HV) single crystal is shown in Figure 4. In this figure, the meridian is the lamellar stacking direction in the sedimented mats. Well-resolved fiber diffraction patterns of P(3HB) α-form,[34] in which all reflections are arced, were observed for all copolymer samples. As indexed in Figure 4a, the 020, 110, and 200 reflections were recognized at $2\theta = \sim 7.8°$, 10.0°, and 16.7° on the equatorial line (*a**- and *b**-axes) and the 002 reflection at about $2\theta = \sim 18.9°$ on the meridional line (*c**-axis). The far right WAXD pattern in a series of images for each sample was taken just before the complete melting. The intensities of the reflections obviously reduced compared with the other patterns.

The plots of crystallinity, X_c, against T_a, extracted from the 2D WAXD patterns, are shown in Figure 5. For convenience, to provide the relation between the changes in crystallinity and heat evolution, the differentiation of X_c with respect to T_a (dX_c/dT_a) and DSC thermogram are also shown in this figure. This figure is also classified into three regions for comparison with the SAXS results. It is noted that the X_c represents the relative value to that at room temperature. As can be seen in this figure, the change of crystallinity is always accompanied by the heat evolution. In region I, both behaviors remain unchanged. In region II, the dX_c/dT_a decreases and then increases, corresponding to the lower endotherm and the exotherm-like signals of DSC, indicating that the discontinuous lamellar thickening observed by SAXS is caused by melting of original crystals and subsequent recrystallization. In region III, the X_c drops finally to zero, which is evidently associated with the complete melting of reorganized crystals.

We reported previously that the recovery of crystallinity after the partial melting falls with increasing the initial lamellar thickness for P(3HB) homopolymer.[22] This is because the crystallization following the melting at high temperatures progresses slowly owing to low supercoolings. Figure 5 shows that, with increasing 3HV content, the first decrease of X_c is more profound, whereas the melting of original crystals occurs at lower temperatures. Bloembergen et al. and Scandola et al. have revealed that the crystallization rate of P(3HB-*co*-3HV) decreases with increasing 3HV unit.[24,28] This means that the accommodation of 3HV unit with longer side chain than 3HB unit in the crystal lattice is basically difficult. It is thus considered that the profound drop in X_c for high 3HV content is caused by the difficulty of chain arrangement in the recrystallization process.

The temperature dependence of unit lattice dimensions (*a*-, *b*-, and *c*-axes) was estimated from the peak positions of 200, 020, and 002 reflections in Figure 4. Figure 6 shows the plots of *a*-, *b*-, and *c*-axes against T_a. These parameters were obtained on the assumption that the unit cell is orthorhombic[34] at the temperatures investigated here. The lattice parameters increased gradually due to thermal expansion in region I, then reduced slightly in region II, and finally showed the tendency to increase or constant in region III. This temperature dependence of these dimensions is almost the same as that in P(3HB) homopolymer.[21,22]

The unit lattice dimensions, especially *a*- and *b*-axes, at room temperature increased with increasing 3HV unit, indicating that the 3HV units are incorporated in the lamellar crystal as reported previously.[25−30] For P(3HB) single crystals, the maxima of these parameters were recognized near the boundary between regions I and II. The lamellar thickening of P(3HB) single crystal results in the contraction of the apparent unit cell parameters.[21,22] The same behavior has been also observed in the case of ultralong alkanes.[14] For the copolymer single crystals investigated here, however, the maxima were recognized at far lower temperatures below the boundary. An annealing temperature where the maxima of *a*- and *b*-axes were observed decreased with increasing 3HV unit. This reason is unclear, but the stability of crystals might be improved by the elimination of the distortion of chain conformation or of crystal lattice at the vicinity of 3HV unit prior to lamellar thickening, and as a result the apparent contraction might occur.

The change of *c*-axis from slight expansion to contraction lagged behind those of *a*- and *b*-axes. The behavior of *c*-axis corresponded rather strictly to the discontinuous increase of long period. The increase in chain stem length may bring about the apparent contraction in *c*-axis.[21,22] Interestingly, the degree of contraction decreased with increasing 3HV unit. This might be due to incomplete reorganization as will be discussed below in detail.

The annealing temperature dependence of apparent crystallite sizes (D_{200}, D_{020}, and D_{002}) was investigated. Figure 7 shows the plots of D_{200}, D_{020}, and D_{002} against T_a. The temperature dependence of these sizes is the same as that in P(3HB) homopolymer.[21,22] The D_{200} and D_{020} gradually increased, and

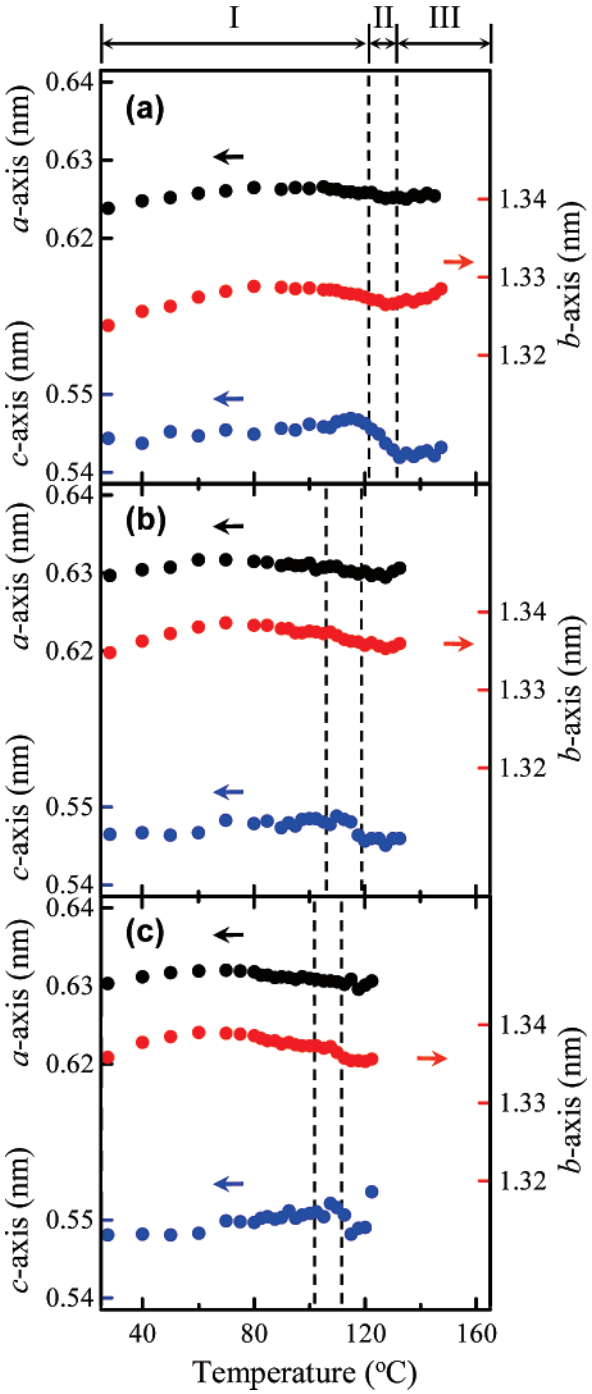

Figure 6. Lattice dimension as a function of temperature: (a) 5.3, (b) 10.9, and (c) 16.0 mol % 3HV.

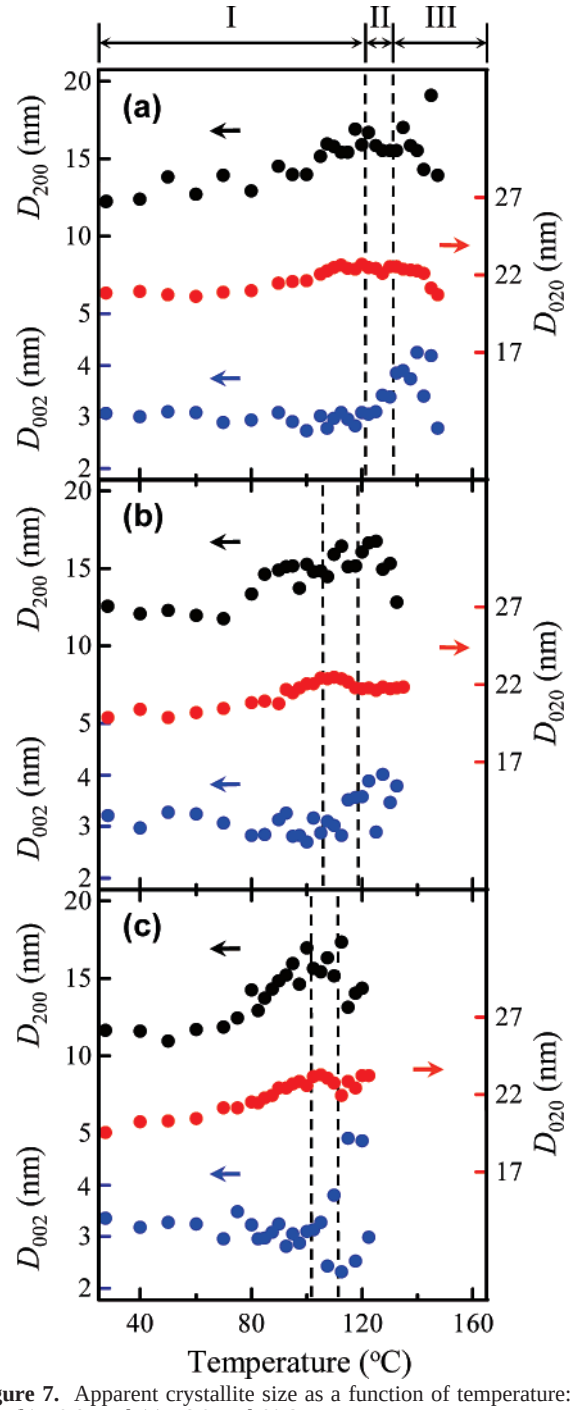

Figure 7. Apparent crystallite size as a function of temperature: (a) 5.3, (b) 10.9, and (c) 16.0 mol % 3HV.

the D_{002} remained almost constant in region I. The D_{200} and D_{020} almost remained constant in regions II and III. It is noteworthy that the D_{002}, which corresponds to the chain stem length, starts to increase from region II. This behavior is related directly to the discontinuous increase in long period observed by SAXS (see Figures 1−3), suggesting that the discontinuous increase of the long period is accompanied by not only the formation of amorphous layer but also the real thickening of crystal.

There is another noticeable point in the effect of 3HV unit on D_{002}. There was little difference in D_{002} among as-grown crystals of copolymers whereas the lamellar thickness increased with the content of 3HV. Similarly, the D_{002} of reorganized crystals depended little on the content of 3HV unit, whereas the long period of reorganized crystal increased with increasing 3HV content. These facts indicate that 3HV units are partly accommodated in the folding parts of chains in both the original and the reorganized crystal.[26,27,29,30] In addition, whereas the copolymers with high 3HV content formed the thick lamellae or D_{002} of the resulting crystals was almost the same among all copolymers, the transition temperature obviously depressed with increasing 3HV content. This supports that the other 3HV units is included into the crystal lattice.[26,27,29,30]

Thickening Mechanism of P(3HB-*co*-3HV) Single Crystals. If the single crystal of P(3HB-*co*-3HV) thickens by sliding diffusion of chains through the crystal lattice, the 3HV units that exist in the folding parts are inevitably pulled into the lattice due to chain translation. In this case, the jump of thickening is likely suppressed with increasing 3HV content because the longer side chain of the 3HV unit is certain to hinder the

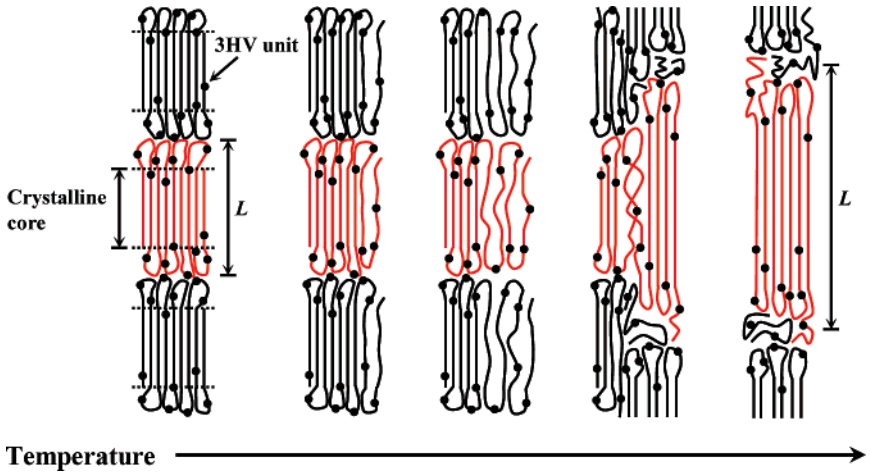

Figure 8. Schematic representation of thickening mechanism of P(3HB-*co*-3HV) single crystals in the transition region. L = long period. The dot represents the 3HV unit.

translation. However, such behavior was not recognized in the present SAXS result (see Figure 3). We can thus imagine that the discontinuous thickening of P(3HB-*co*-3HV) single crystal is caused by melting and recrystallization rather than the chain sliding diffusion mechanism.

A schematic illustration of thickening behavior of P(3HB-*co*-3HV) single crystals on heating is shown in Figure 8. In this figure, the black dot represents the 3HV unit. Many of the 3HV units are anticipated to exist in the folding part and the rest in the P(3HB) crystal lattice.[26,27,29,30] For the sedimented mats of solution grown single crystals, the single crystals are regularly stacked along the chain direction. When the crystals are heated, the lamellar thickening occurs discontinuously at a T_a. But the melting is not complete one that helical chains relax into random coil state,[20] as shown in Figure 8, taking account into the experimental evidence that subsequent recrystallization takes place immediately and that the chain axis direction maintains before and after the reorganization as revealed by the present 2D SAXS and WAXD patterns. It is deduced that the chains or chain segments detached from the lattice might be in an intermediate state which is not crystalline order. Such chain segments possibly diffuse mutually to the space in which the adjacent crystals existed.[22] Namely, the discontinuous lamellar thickening of the crystal is a cooperative process with the adjacent crystals along the stacking direction as shown in Figure 8.

However, some chains or segments are not incorporated to the crystal lattice, and the extent increases with increasing 3HV content. These further relax and remain as random coil and tie chain between the reorganized crystals, loose loop, cilia, and so on. The continuous increases of long period after the discontinuous lamellar thickening is mainly associated with the increase of amorphous phases by melting of reorganized crystal rather than the increase of fold period.[33]

Concluding Remarks

P(3HB-*co*-3HV) single crystals with various composition of 3HV were grown isothermally at 60 °C in a dilute 1-octanol solution. Structural changes of the sedimented single-crystal mats on heating were followed by real-time synchrotron radiation SAXS and WAXD in order to investigate the effect of 3HV unit on the structural changes during annealing. The 2D SAXS measurement revealed that P(3HB-*co*-3HV) single crystal exhibits a discontinuous increase in long period as well as single crystal of P(3HB) homopolymer. The discontinuous increase was recognized in the temperature range of several degrees, indicating that the two populations with different thickness coexist. It was found that the jump of lamellar thickness is not hindered by 3HV units. The lamellar thickening started at lower temperatures with increasing 3HV unit because the 3HV unit causes the reduction in the thermal stability of the original crystal, that is, in the interaction between the chain stems. The changes in crystallinity and thermal property during the discontinuous thickening are associated with melting and recrystallization. By revealing the effect of second monomer unit, we could provide that the discontinuous lamellar thickening of P(3HB) single crystal proceeds by the mechanism of partial melting and subsequent recrystallization.

Acknowledgment. This work has been partly supported by grants of Ecomolecular Science Research from RIKEN Institute, SORST of Japan Science and Technology Agency (JST), by a DRI Director's Grant from RIKEN Institute (to M.F.), and a Grant-in-Aid for Young Scientists (A) from the Ministry of Education, Culture, Sports, Science and Technology of Japan (No. 15685009) (to T.I.). The authors also thank Yamamoto-seisakujo, Japan, and KEYENCE Co. Ltd., for making the sample heat device and its remote control unit, respectively.

References and Notes

(1) Dreyfuss, P.; Keller, A. *J. Macromol. Sci., Phys.* **1970**, *B4*, 811−836.
(2) Mandelkern, L.; Sharma, R. K.; Jackson, J. F. *Macromolecules* **1969**, *2*, 644−647.
(3) Tian, M.; Loos, J. *J. Polym. Sci., Part B: Polym. Phys.* **2001**, *39*, 763−770.
(4) Fujita, M.; Iwata, T.; Doi, Y. *Polym. Degrad. Stab.* **2003**, *81*, 131−139.
(5) Magonov, S. N.; Yerina, N. A.; Ungar, G.; Reneker, D. H.; Ivanov, D. A. *Macromolecules* **2003**, *36*, 5637−5649.
(6) Fujita, M.; Doi, Y. *Biomacromolecules* **2003**, *4*, 1301−1307.
(7) Nakamura, J.; Kawaguchi, A. *Macromolecules* **2004**, *37*, 3725−3734.
(8) Organ, S. J.; Hobbs, J. K.; Miles, M. J. *Macromolecules* **2004**, *37*, 4562−4572.
(9) Zhai, X.-M.; Wang, W.; Ma, Z.-P.; Wen, X.-J.; Yuan, F.; Tang, X.-F.; He, B.-L. *Macromolecules* **2005**, *38*, 1717−1722.
(10) Rastogi, S.; Spoelstra, A. B.; Goossens, J. G. P.; Lemstra, P. J. *Macromolecules* **1997**, *30*, 7880−7889.
(11) Rastogi, S.; Kurelec, L.; Lemstra, P. J. *Macromolecules* **1998**, *31*, 5022−5031.
(12) Ungar, G.; Zeng, X. *Chem. Rev.* **2001**, *101*, 4157−4188.
(13) de Silva, D. S. M.; Zeng, X.; Ungar, G.; Spells, S. J. *Macromolecules* **2002**, *35*, 7730−7741.
(14) Terry, A. E.; Phillips, T. L.; Hobbs, J. K. *Macromolecules* **2003**, *36*, 3240−3244.
(15) Krüger, K. N.; Zachmann, H. G. *Macromolecules* **1993**, *26*, 5202−5208.

(16) Wang, Z. G.; Wang, X. H.; Hsiao, B. S.; Phillips, R. A.; Medellin-Rodriguez, F. J.; Srinivas, S.; Wang, H.; Han, C. C. *J. Polym. Sci., Part B: Polym. Phys.* **2001**, *39*, 2982−2995.
(17) Organ, S. J.; Li, J.; Terry, A. E.; Hobbs, J. K.; Barham, P. J. *Polymer* **2004**, *45*, 8925−8936.
(18) Li, J.; Organ, S. J.; Terry, A. E.; Hobbs, J. K.; Barham, P. J. *Polymer* **2004**, *45*, 8937−8947.
(19) Kovacs, A. J.; Straupe, C. *Faraday Discuss. Chem. Soc.* **1979**, *68*, 225−238.
(20) Kawaguchi, A.; Murakami, S.; Kajiwara, K.; Katayama, K. *J. Polym. Sci., Part B: Polym. Phys.* **1989**, *27*, 1463−1476.
(21) Fujita, M.; Sawayanagi, T.; Tanaka, T.; Iwata, T.; Abe, H.; Doi, Y.; Ito, K.; Fujisawa, T. *Macromol. Rapid Commun.* **2005**, *26*, 678−683.
(22) Sawayanagi, T.; Tanaka, T.; Iwata, T.; Abe, H.; Doi, Y.; Ito, K.; Fujisawa, T.; Fujita, M. *Macromolecules* **2006**, *39*, 2201−2208.
(23) Doi, Y. *Microbial Polyesters*; VCH: New York, 1990.
(24) Bloembergen, S.; Holden, D. A.; Hamer, G. K.; Bluhm, T. L.; Marchessault, R. H. *Macromolecules* **1986**, *19*, 2865−2871.
(25) Bluhm, T. L.; Hamer, G. K.; Marchessault, R. H.; Fyfe, C. A.; Veregin, R. P. *Macromolecules* **1986**, *19*, 2871−2876.
(26) Mitomo, H.; Barham, P. J.; Keller, A. *Sen-i Gakkaishi* (*Jpn.*) **1986**, *42*, 589−596.
(27) Mitomo, H.; Barham, P. J.; Keller, A. *Polym. J.* **1987**, *19*, 1241−1253.
(28) Scandola, M.; Ceccorulli, G.; Pizzoli, M.; Gazzano, M. *Macromolecules* **1992**, *25*, 1405−1410.
(29) Mitomo, H.; Doi, Y. *Int. J. Biol. Macromol.* **1999**, *25*, 201−205.
(30) Yoshie, N.; Saito, M.; Inoue, Y. *Macromolecules* **2001**, *34*, 8953−8960.
(31) Yoshie, N.; Menju, H.; Sato, H.; Inoue, Y. *Macromolecules* **1995**, *28*, 6516−6521.
(32) Kumaraswamy, G.; Verma, R. K.; Kornfield, J. A.; Yeh, F.; Hsiao, B. S. *Macromolecules* **2004**, *37*, 9005−9017.
(33) Cho, M. H.; Kyu, T.; Lin, J. S.; Saijo, K.; Hashimoto, T. *Polymer* **1992**, *33*, 4152−4157.
(34) Yokouchi, M.; Chatani, Y.; Tadokoro, H.; Teranishi, K.; Tani, H. *Polymer* **1973**, *14*, 267−272.

MA062957D